Numerical simulation of mesoscopic systems with open boundaries using the multidimensional time-dependent Schrödinger equation

Leonard F. Register, Umberto Ravaioli, and Karl Hess
Beckman Institute and Coordinated Science Laboratory, University of Illinois at Urbana-Champaign, Urbana, Illinois 61801

(Received 11 December 1990; accepted for publication 7 February 1991)

A numerical procedure based on the time-dependent Schrödinger equation for the modeling of multidimensional mesoscopic devices is presented. The primary features of this numerical method are a tight-binding formulation of the quantum mechanical Hamiltonian, an alternating direction implicit generalization of the Crank–Nicholson method for solving the discretized multidimensional time-dependent Schrödinger equation, and a numerical implementation of absorbing boundary conditions for propagating wavefunctions at the open boundaries of the simulated region. To show the capabilities of the absorbing boundary scheme, numerical results are presented for the diffusion of localized wavepackets out of open simulation regions. As an application to mesoscopic systems, results are presented for the switching in a T-structure quantum modulated transistor with a continuous input wavefunction.

I. INTRODUCTION

The transient behavior of one-dimensional quantum devices, such as the resonant tunneling diode, often is simulated using numerical Wigner function methods.[1,2] This technique is appealing because the Wigner distribution function can be regarded to some extent as the quantum equivalent of a classical distribution function. However, since both spatial coordinates and momentum are simultaneously considered, for the simulation of an n-dimensional structure the Wigner function is $2n$-dimensional. Thus, the simulation of novel quantum devices, such as the T-structure[3] and Aharonov–Bohm effect[4] transistors, quickly becomes prohibitive using the Wigner function approach because at least two spatial dimensions must be included in the simplest models. An alternative approach is the direct solution of the n-dimensional Schrödinger equation. While a summation over incident states is required, this summation will be limited in many cases. In this paper a numerical method suitable for the solution of the multidimensional time-dependent Schrödinger equation in mesoscopic structures is presented. To provide an unambiguous treatment of quantum mechanics for the spatially discretized coordinate system that must be employed, a tight-binding formalism is used. To ensure stability and unitary time evolution of the wavefunction, a half-implicit Crank–Nicholson scheme is employed. To allow simulation of transport through device structures, absorbing boundary conditions are included within this scheme. Results are presented first for the diffusion of localized wavepackets out of the open simulation regions, to demonstrate boundary absorption of transient current flow. Then results are presented for switching in a T-structure quantum modulated transistor, where the quantum interference pattern of the wavefunction is varied by changing the effective length of a side arm in a quantum wire. In this last example, in addition to boundary absorption, a continuous incoming wavefunction is included in the boundary conditions.

II. NUMERICAL APPROACH

A. Discretization of Schrödinger's equation

The time evolution of the spatially and temporally continuous carrier wavefunction $\psi(\mathbf{r},t)\equiv\langle\mathbf{r}|\psi(t)\rangle$ is emulated by that of a discretized wavefunction $\langle\mathbf{R}|\psi(t_n)\rangle$ on a uniform virtual tight-binding lattice. The tight-binding Hamiltonian used here is of the form[5]

$$H=\sum_{\mathbf{R}}|\mathbf{R}\rangle\epsilon_{\mathbf{R}}\langle\mathbf{R}| + \sum_{\mathbf{R},\mathbf{j}}(|\mathbf{R}\rangle\nu\langle\mathbf{R}+\hat{\mathbf{j}}\Delta| + |\mathbf{R}\rangle\nu\langle\mathbf{R}-\hat{\mathbf{j}}\Delta|), \quad (1)$$

where $\mathbf{R}$ are the lattice sites, Δ is the lattice spacing, $\hat{\mathbf{j}}$ are the set of orthogonal unit vectors of the multidimensional space, and $\mathbf{R}\pm\hat{\mathbf{j}}\Delta$ are the corresponding nearest neighbor sites, as depicted in Fig. 1. The "hopping potential" ν and the site potentials $\epsilon_{\mathbf{R}}$ are defined by

$$\nu\equiv-\hbar^2/2m^*\Delta^2 \quad (2)$$

and

$$\epsilon_{\mathbf{R}}\equiv-\sum_{\mathbf{j}}2\nu+V(R), \quad (3)$$

respectively, where $V(\mathbf{R})$ is the potential energy. Thus, by applying this tight-binding Hamiltonian to the wavefunction $\langle\mathbf{R}|\psi\rangle$, with the condition $\langle\mathbf{R}|\mathbf{R}'\rangle\equiv\delta_{\mathbf{R},\mathbf{R}'}$, one obtains

$$\langle\mathbf{R}|H|\psi\rangle=-\frac{\hbar^2}{2m^*\Delta^2}\sum_{\mathbf{j}}(\langle\mathbf{R}+\hat{\mathbf{j}}\Delta|\psi\rangle-2\langle\mathbf{R}|\psi\rangle + \langle\mathbf{R}-\hat{\mathbf{j}}\Delta|\psi\rangle)+V(\mathbf{R})\langle\mathbf{R}|\psi\rangle. \quad (4)$$

This result is equivalent to a uniform mesh finite difference discretization of the continuum effective mass Hamiltonian $H=(\hbar^2/2m^*)\nabla^2+V(\mathbf{r})$. The tight-binding formalism is used here because it provides an unambiguous treatment of quantum mechanics for the spatially discretized system that must be employed, and because it provides compati-

 0021-8979/91/107153-06$03.00

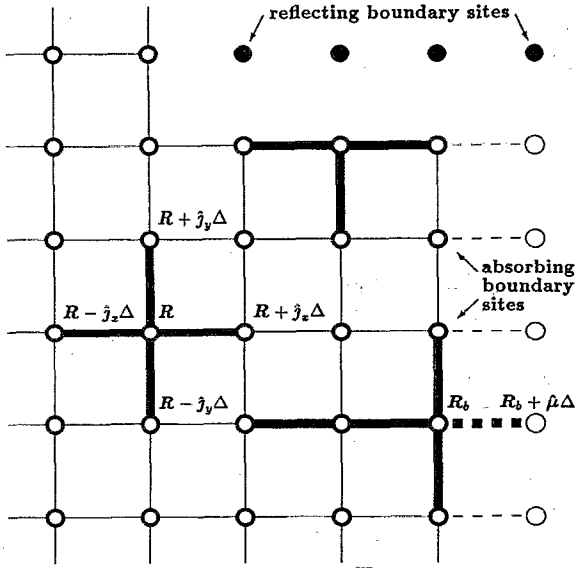

FIG. 1. Simulation region of the virtual tight-binding lattice showing the coupling of sites to their neighbors. Departures from the nearest-neighbor coupling, Eq. (1), occur at the boundaries, particularly for the absorbing boundaries where complicated coupling patterns may result from the extrapolation schemes of Eqs. (8)–(10).

bility with a previously developed Green's function method for calculating steady-state transmission coefficients.[6] As will be shown later, inconsistent approximations of the continuum are a potential source of error in absorbing boundary conditions.

It is known that a Crank–Nicholson approach should be used for stability and preservation of the wavefunction norm, when a first order forward difference is used for the time discretization of the Schrödinger's equation.[7] The Hamiltonian is approximated by the average between the current and the next time-step value, yielding the half-implicit discretized equation

$$i\hbar\frac{|\psi(t_n+\Delta t)\rangle - |\psi(t_n)\rangle}{\Delta t} = \frac{H|\psi(t_n)\rangle + H|\psi(t_n+\Delta t)\rangle}{2} \tag{5}$$

where Δt is the time step. For multidimensional calculation, however, large matrices are generated. To avoid this complication, the space operator can be split into components and an alternating direction implicit (ADI) approach[8,9] employed. Specifically, in two-dimensions (2-D), two subiterations with time-step $\Delta t/2$ are used,

$$\begin{aligned} i\hbar|\psi(t_n+\tfrac{1}{2}\Delta t)\rangle &= i\hbar|\psi(t_n)\rangle + \tfrac{1}{4}\Delta t[H_x|\psi(t_n+\tfrac{1}{2}\Delta t)\rangle \\ &\quad + H_y|\psi(t_n)\rangle] \\ i\hbar|\psi(t_n+\Delta t)\rangle &= i\hbar|\psi(t_n+\tfrac{1}{2}\Delta t)\rangle + \tfrac{1}{4}\Delta t[H_x|\psi(t_n+\tfrac{1}{2}\Delta t)\rangle \\ &\quad + H_y|\psi(t_n+\Delta t)\rangle], \end{aligned} \tag{6}$$

where H_x and H_y result from the decomposition of the tight-binding Hamiltonian of Eq. (1) into its orthogonal components. The structure of the scheme is given in (6) reveals that the x- and y-components are alternatively implicit in the two subiterations. This procedure requires only the solution of tridiagonal matrices along the horizontal or vertical mesh lines. Furthermore, since such sets of matrix solutions are decoupled from each other, a very efficient implementation on a supercomputer is possible.

B. Absorbing boundary conditions

Realistic modeling of mesoscopic devices requires simulation of both open and closed boundaries. Numerical simulation of closed (reflecting) boundaries is straightforward; the coupling potential v to the boundary tight-binding lattice sites simply can be reset to zero, or equivalently the boundary wavefunctions fixed at zero. The challenge here, a challenge common to all fields concerned with wave propagation,[10] is numerical simulation of outflow of wavefunctions through the simulation region open boundaries without introducing spurious reflections due to the numerical scheme. The work of Mains and Haddad in one-dimension (1-D)[11,12] suggests that a curve-fitting approach for the wavefunction near the open boundaries may provide a solution to this problem. They approximate the boundary wavefunctions as

$$\begin{aligned} \psi_{\text{left}}(x) &\simeq ae^{ikx} + (b_l + c_l x)e^{-kx} \\ \psi_{\text{right}}(x) &\simeq (b_r + c_r x)e^{k'x} \end{aligned} \tag{7}$$

and then apply the continuum Hamiltonian to calculate the time evolution of the wavefunction at the boundary. Here, k is the wavevector of a left incoming monochromatic wave, k' is the corresponding wavevector at the right-hand side boundary with an allowance for the potential energy difference between the boundaries, and the coefficients b and c are obtained from a linear fit to the wavefunction at the boundary and first internal points of the discrete simulation grid employed. This method was effective for their 1-D simulations of resonant tunneling structures. However, this boundary condition loses accuracy as the relative variation in the wavefunction momentum from the specified monochromatic limit increases.[13] Furthermore, the application of the continuum Hamiltonian to the boundary wavefunctions of Eq. (7) is inconsistent with the finite difference discretization of the Hamiltonian used within the domain. A discrepancy exists between the parabolic band structure of the continuum Hamiltonian and the tight-binding band structure implicit to the finite difference discretization. This discrepancy is particularly significant for large wavevectors.

In this paper a more general and robust approach to fitting the boundary wavefunction and evaluating the boundary Hamiltonian is presented. The wavefunction is extrapolated on the tight-binding lattice sites immediately outside the open boundaries using

$$\langle \mathbf{R}_e|\psi(t)\rangle \simeq \Gamma[\langle \mathbf{R}|\psi(t_n)\rangle]\gamma\left[\frac{\langle \mathbf{R}|\psi(t)\rangle}{\langle \mathbf{R}|\psi(t_n)\rangle}\right], \tag{8}$$

or, similarly,

$$\langle \mathbf{R}_e|\psi(t)\rangle \simeq \Gamma[\langle \mathbf{R}|\psi(t_n)\rangle] + \gamma[\langle \mathbf{R}|\psi(t)\rangle$$

$$- \langle \mathbf{R} | \psi(t_n) \rangle], \tag{9}$$

where $\mathbf{R}_e$ is an external lattice site, and Γ and γ are independent extrapolation functions. For the 2-D ADI scheme (6), $t = t_n + \frac{1}{2}\Delta t$ or $t = t_n + \Delta t = t_{n+1}$. The tight-binding Hamiltonian of Eqs. (1)–(4) then is applied to the boundary sites, just as it is applied to the internal sites, to obtain the time evolution of the boundary wavefunction, as depicted in Fig. 1. Inclusion of specified incoming wavefunctions $\langle \mathbf{R} | \psi_i \rangle$ in the boundary conditions is accomplished by replacing $\langle \mathbf{R}_{(e)} | \psi \rangle$ in Eqs. (8) and (9) with $\langle \mathbf{R}_{(e)} | \psi \rangle - \langle \mathbf{R}_{(e)} | \psi_i \rangle$. Further, both of the extrapolation schemes Γ and γ can be varied as a function of $\mathbf{R}_e$ and t_n if required.

The separation of the extrapolation schemes of Eqs. (8) and (9) into the components Γ (explicit) and γ (implicit) is intended to satisfy two conflicting requirements: Accuracy of the extrapolation and realizability of the implicit scheme (6). Because the primary extrapolation Γ is performed only explicitly, complicated extrapolation schemes can be used without reducing the efficiency of the ADI numerical approach described in Sec. II A above. This flexibility allows complicated admixtures of propagating and evanescent states to be fit at the boundaries.[14,15] On the other hand, γ is required to extrapolate only small changes in the boundary wavefunction over the time step and thus, extrapolation schemes that can be readily evaluated implicitly are sufficient. Also, here there is no inherent restriction on the nature of the incoming wavefunction; $\langle \mathbf{R} | \psi_i \rangle$ can be monochromatic or otherwise, e.g., a propagating wavepacket. In contrast, in Refs. 11 and 12 the incoming wavefunction is necessarily monochromatic. Finally, application of the tight-binding Hamiltonian of Eqs. (1)–(4) to the boundary lattice sites as to the internal sites allows no possibility of discrepancy in the resulting energy band structure between the two sets of lattice sites.

For the example calculations presented in the next section, we chose the following simple scheme, in the form of Eq. (8):

$$\langle \mathbf{R}_b + \hat{\mu}\Delta | \psi(t_n) \rangle \simeq \left[\prod_{n=0}^{N} \langle \mathbf{R}_b - \hat{\mu} n\Delta | \psi(t_n) \rangle^{a_n} \right] \times \left[\sum_{n=0}^{N} a_n \frac{\langle \mathbf{R}_b - \hat{\mu} n\Delta | \psi(t) \rangle}{\langle \mathbf{R}_b - \hat{\mu} n\Delta | \psi(t_n) \rangle} \right] \tag{10}$$

where $\mathbf{R}_b$ is the boundary site and $\hat{\mu}$ is a unit vector normal to the boundary and directed outwards, as shown in Fig. 1. An appropriate choice of the coefficients a_n provides any desired polynomial curve fit near the boundary. For example, for a linear curve fit, $a_0 = 2$, $a_1 = -1$, $a_{n>2} = 0$, and for a parabolic curve fit, $a_0 = 3$, $a_1 = -3$, $a_2 = 1$, $a_{n>3} = 0$. In addition, to prevent the "absorbing" boundaries from inadvertently becoming probability sources, probability flow from an external lattice site to a boundary site has been restricted. It can be shown readily that

$$\frac{d}{dt} |\langle \mathbf{R} | \psi \rangle|^2 = \frac{2\nu}{\hbar} \sum_{\mathbf{j}} \mathrm{Im}[\langle \psi | \mathbf{R} \rangle \langle \mathbf{R} + \hat{\mathbf{j}}\Delta | \psi \rangle + \langle \psi | \mathbf{R} \rangle \langle \mathbf{R} - \hat{\mathbf{j}}\Delta | \psi \rangle] \tag{11}$$

for the tight-binding formalism used here. Therefore, should the phase of $\Gamma(\langle \mathbf{R} | \psi(t_n) \rangle - \langle \mathbf{R} | \psi_i(t_n) \rangle)$ ever lag that of $\langle \mathbf{R}_b | \psi(t_n) \rangle - \langle \mathbf{R}_b | \psi_i(t_n) \rangle$ for any boundary lattice site, we project the former complex quantity onto the latter to obtain a new prediction Γ of equal phase, with the minimum change to the initial prediction possible.

III. NUMERICAL EXAMPLES

A. Diffusion through absorbing boundaries

The quantum mechanical diffusion of localized wavepackets out of open regions has been simulated to demonstrate the effectiveness of the absorbing boundary scheme presented here. Because of the wide spectral spread in energies, small mean momentums, and open boundaries on all sides, these diffusion examples pose in many respects a difficult numerical challenge. For the first such example, the diffusions of two identical stationary Gaussian wavepackets out of concentric square domains were simulated and the results compared, as shown in Figs. 2(a) and 2(b). Here, the probability distribution $|\langle \mathbf{R} | \psi \rangle|^2$ obtained for the smaller domain is overlaid on that obtained for the larger to facilitate comparison. The difference between the two results at the boundary of the inner region is a measure of the error induced by the application of absorbing boundary conditions of Eq. (10) with, in this case, a cubic curve fit. After 200 fs of simulation such error remained negligible, as to be expected; for the primary extrapolation Γ, a parabolic or higher order curve fit is exact for a Gaussian wavepacket. In this and all following examples the effective mass m^* of GaAs ($0.067 m_e$), a tight-binding grid spacing Δ of 10 Å and a time-step Δt of 1.0 fs were used. For comparison, for the wavefunction of this example, which has zero mean momentum (and no reference incoming wavefunction), the absorbing boundary condition in Refs. 11 and 12 becomes, in effect, a reflecting condition as the continuum Hamiltonian vanishes at the boundary, allowing no time evolution of the wavefunction there.

For the second example, the diffusions of identical wavefunctions, each this time initially a sum of two Gaussian wavepackets with a relative phase difference of $\pi/2$ radians, out of two concentric rectangular domains were simulated and compared, as shown in Figs. 2 (c) and 2(d). In these simulations, the curve fit of Eq. (10) was no longer exact, and one can notice small discrepancies between the two solutions at the inner boundary after 200 fs of simulation. The error exhibited in Fig. 2(d), however, is emphasized by the choice of scale which is 50 times smaller than in Fig. 2(c).

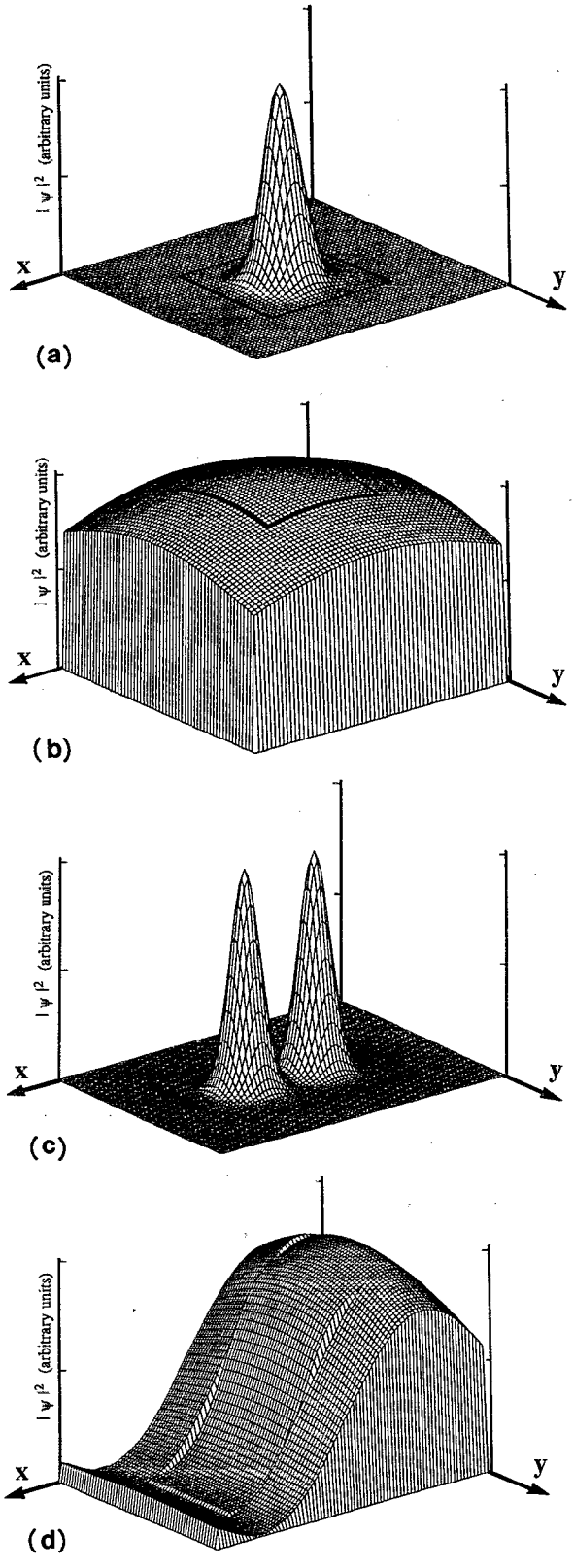

FIG. 2. Simulation results for the diffusions of Gaussian wavepackets out of concentric open regions: (a) initial probability distribution and (b) probability distribution after 200 fs, for a single stationary Gaussian wavepacket; and (c) initial probability distribution, and (d) probability distribution after 200 fs, for a wavefunction obtained from the sum of two Gaussian wavepackets with a relative phase difference of $\pi/2$ radians. The boundaries of the inner regions are outlined when not otherwise apparent.

B. Switching of a quantum interference structure

As a final example, the 2-D numerical scheme presented here was used to simulate the switching transient in a T-structure quantum modulated transistor.[3] An idealized 2-D structure delimited by hard walls was assumed to allow comparison of the results obtained here with steady-state transmission coefficients obtained using the steady-state Greens function method of Ref. 6. However, this assumption does not reflect a limitation of the method; finite potential walls could have been modeled via the spatially varying site potentials of Eq. (3). The input and output leads of the structure were modeled as quantum wires with a width W of 100 Å. The side arm had the same width and an initial length L of 70 Å. Again, the boundary conditions of Eq. (10) were used, though this time a simple linear curve fit proved sufficient. However, an incoming wavefunction $\langle \mathbf{R}|\psi_i\rangle \propto \chi(Y)\exp(ikX)$ was included in the left boundary condition. Here, $\chi(Y)$ is the ground state transverse wavefunction of the lead and k is the incident momentum wavevector taken to be $2\pi/200$ Å^{-1}. The initial steady-state probability distribution $|\langle \mathbf{R}|\psi\rangle|^2$ is shown in Fig. 3(a). Due to quantum interference effects in the stub region, the transmission probability through the structure was nearly zero. One can see a pronounced peak of probability inside the stub region, and a standing wave pattern in the input lead indicating nearly total reflection. The time evolution of the probability distribution after switching the stub length from 70 to 100 Å is shown in Figs. 3(b)–3(i). Here, a uniform probability scale is maintained throughout. The transient exhibits a quick collapse of the probability peak in the stub and a corresponding wavefront in the output lead. The decrease of the reflected wave in the input lead is evident from the progressive reduction of the standing wave pattern. By 500 fs the structure was clearly *on* with a transmission probability near unity, with only a hint of reflection at the input noticeable from the weak standing wave pattern. Only a small fraction of the original probability peak inside the stub remained. Beyond this time, although switching was complete, the time evolution still exhibited small persistent oscillations. The abrupt initial switching excited localized eigenstates of the stub at various energies. These eigenstates, which are evanescent in the leads, did not decay in time since dissipation is not included in the model, and thus continued to beat against the propagating state. If desired, such localized states can be filtered out by Fourier transforming from time to energy at the energy of the incident wave. Indeed, this approach was used to obtain the initials conditions for this simulation, Fig. 3(a), after switching from a simple quantum wire with no stub. On the other hand, localized states can be isolated by Fourier transforming at their energies. The simulation results were not appreciably affected by changing the lengths of the leads to check the absorbing boundary conditions. A similar simulation of switch-off exhibited a somewhat quicker and less oscillatory switching characteristic. In both cases, the steady-state transmission probabilities obtained here are identical to those obtained using the steady-state Green's function method of Ref. 6.

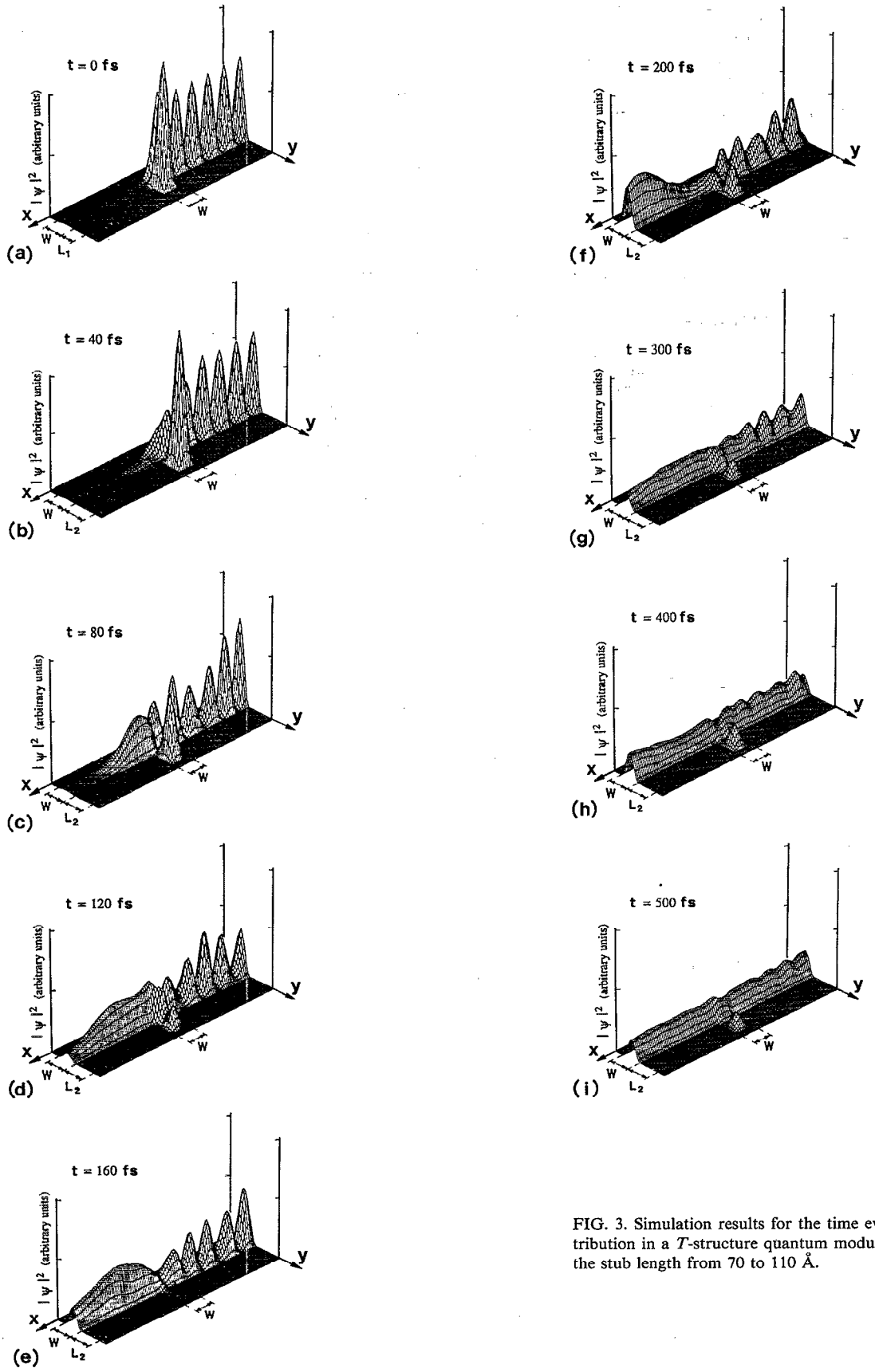

FIG. 3. Simulation results for the time evolution of the probability distribution in a T-structure quantum modulated transistor after switching the stub length from 70 to 110 Å.

IV. CONCLUSIONS

We have presented a numerical method based on the time-dependent Schrödinger equation and incorporating absorbing boundary conditions, suitable for the simulation of transient response in multidimensional mesoscopic devices. We have shown results for the diffusion of localized

wavepackets out of open systems and for the switching of a T-structure quantum modulated transistor. Statistical distributions in the state occupancy in the contact reservoirs can be included by a weighted sum of results for monochromatic incident states over the appropriate energy range. Future work includes the introduction of potential energy self-consistency, via the solution of Poisson's equation, and of a spatially varying effective mass.

ACKNOWLEDGMENTS

This work was supported by the U.S. Army Research Office, the National Science Foundation, and the National Center for Computational Electronics. Computer time on the CRAY X-MP of the National Center for Supercomputing Applications of the University of Illinois was made available by a grant from CRAY Research, Inc.

[1] U. Ravaioli, M. A. Osman, W. Pötz, N. Kluksdahl, and D. K. Ferry, Physica B **134**, 36 (1985).
[2] W. R. Frensley, Phys. Rev. B **36**, 1570 (1987).
[3] F. Sols, M. Macucci, U. Ravaioli, and K. Hess, Appl. Phys. Lett. **54**, 350 (1989).
[4] S. Datta, M. Melloch, S. Bandyopadhyay, R. Noren, M. Vaziri, M. Miller, and R. Reifenberger, Phys. Rev. Lett. **55**, 2344 (1985).
[5] E. N. Economou, *Green's Functions in Quantum Physics* (Springer, Berlin, 1983).
[6] F. Sols, M. Macucci, U. Ravaioli, and K. Hess, J. Appl. Phys. **66**, 3892 (1989).
[7] A. Goldberg, H. M. Schey, and J. L. Schwartz, Am. J. Phys. **35**, 177 (1967).
[8] M. Cahay, J. P. Kreskovsky, and H. L. Grubin, Solid- State Electron. **32**, 1185 (1989).
[9] J. R. Barker, in *Nanostructure Physics and Fabrication*, edited by M. A. Reed and W. P. Kirk (Academic, San Diego, CA, 1989), p. 253.
[10] B. Engquist and A. Majda, Math. Comput. **31**, 629 (1977).
[11] R. K. Mains and G. I. Haddad, J. Appl. Phys. **64**, 3564 (1988).
[12] R. K. Mains and G. I. Haddad, J. Appl. Phys. **67**, 591 (1990).
[13] L. F. Register, U. Ravaioli, and K. Hess, in *Computational Electronics: Semiconductor Transport and Device Simulation*, edited by K. Hess, J. P. Leburton and U. Ravaioli (Kluwer, Boston, MA, 1991), p. 235.
[14] D. J. Kirkner, C. S. Lent, and S. Sivaprakasam, Int. J. Numer. Methods Eng. **29**, 1527 (1990).
[15] C. S. Lent and D. J. Kirkner, J. Appl. Phys. **67**, 6353 (1990).